LAWRENCE
LIVERMORE
NATIONAL
LABORATORY

LLNL-JRNL-818277

Integrated Liquid Metal Flowing First Wall and Open-Surface Divertor for Fusion Nuclear Science Facility (FNSF): Concept, Design and Analysis

S. Smolentsev, T. Rognlien, M. Tillack, L. Waganer, C. Kessel

January 11, 2021

Fusion Science and Technology

Disclaimer

LLNL-JRNL-818277

Integrated Liquid Metal Flowing First Wall and Open-Surface Divertor for Fusion Nuclear Science Facility (FNSF): Concept, Design and Analysis

Sergey Smolentsev,[a]* Thomas Rognlien,[b] Mark Tillack,[c] Lester Waganer,[d] Charles Kessel[e]

[a]*University of California, Los Angeles, USA*

[b]*Lawrence Livermore National Laboratory, Livermore, USA*

[c]*University of California, San Diego, USA*

[d]*Consultant, USA*

[e]*Oak Ridge National Laboratory, Oak Ridge, USA*

Abstract - *Within the Fusion Engineering Systems Study (FESS) in the US, the project team is examining the use of liquid metals (LMs) for plasma facing components (PFCs). Our approach has been to utilize an already established fusion design, Fusion Nuclear Science Facility (FESS-FNSF), which is a tokamak-based machine with 518 MW fusion power, a 4.8-m major radius, a 1.2-m minor radius and a machine average neutron wall loading ~ 1 MW/m^2. For this design, we propose a PFC concept that integrates a flowing LM First Wall (FW) and an open-surface divertor. The flowing LM first removes the surface heat flux from the FW and then proceeds to the lower section of the vacuum chamber to form a large area LM surface for absorbing high-peak surface heat flux in the divertor region. In pursuing the application of large open LM surfaces in the FNSF, two new computer codes have been developed and then applied to the analysis of free-surface magnetohydrodynamic (MHD) flows and heat transfer, including fast thin flowing liquid layers over the solid FW ("liquid wall"), a "tub-like divertor" and a "fast flow divertor". The analysis is aimed at optimization of the liquid wall design by matching certain proposed design criteria and also at evaluation of the maximum heat fluxes, using liquid Lithium (Li) as a working fluid. It was demonstrated that the flowing Li FW (at ~ 2 cm and ~ 10 m/s) can tolerate a surface heat flux ~ 1 MW/m^2, while the open-surface Li divertor can remove a maximum high-peak heat flux of 10 MW/m^2. The paper also focuses on the underlying science. One such example is the evaluation and characterization of heat transfer mechanisms and heat transfer intensification in the tub-like Li divertor.*

Keywords - *Plasma facing components, liquid metal, free surface flows, divertor, First Wall, FNSF.*

Note – *Some figures may be in color only in the electronic version.*

---

*E-mail: sergey@fusion.ucla.edu

I. INTRODUCTION

Free-surface LM flows have actively been explored as a promising means for high heat flux removal in fusion cooling applications starting from the late 1980s.[1] Such LM coolants as liquid Li, Sn, SnLi or Ga offer many advantages if compared to other cooling techniques, such as improvements in plasma stability and confinement (when using Li), the capability of high heat/particle flux removal, and elimination of mechanical or thermal stresses compared to solid materials. However, being good electrical conductors, all LMs may suffer from various magnetohydrodynamic (MHD) effects due to interactions between the induced electric currents and a strong plasma-confining magnetic field. Many aspects of LM MHD free-surface flows were analyzed and a few promising designs utilizing free-surface flows proposed in the course of the APEX study in the US (Ref. 2), whose objective was to identify and explore novel concepts for Fusion Chamber Technology that can substantially improve the attractiveness of fusion energy systems. In particular, the APEX study considered liquid walls of either LMs (Li or SnLi) or molten salts (FLiBe or FLiNaBe). In the CliFF concept (Convective Liquid Flow First-Wall) in APEX, a solid FW facing the plasma was eliminated with a thin liquid layer flowing on the plasma side of the FW. Such a layer provides renewable liquid surface immune to radiation damage and largely eliminates thermal stresses and their associated problems in the first structural wall. MHD analysis for CLiFF had shown that the MHD drag (in the case of LMs) might be too high, especially if there is a significant radial magnetic field component – one normal to the free surface. To reduce the MHD forces resulting from the radial magnetic field, it was decided to use insulated poloidal dividers to break strong induced electric currents flowing in the toroidal direction. Also, the APEX study introduced a concept of integrated open-surface divertor, where the streams from the inner and outer FW become the streams of the inner and outer divertor.[3] In the outboard divertor, on the plasma-facing side of the stream, a new design element called a deflector was proposed to redirect the outer FW flow downward to become the outer divertor stream. Such a design was demonstrated to tolerate a peak heat load of 10 MW/m^2 when using molten salt FLiNaBe. In a more recent study (Ref. 4), another approach to handle high heat loads in the divertor region was considered. In this very different LM divertor concept called ACLMD (Actively Convected Liquid Metal Divertor), the divertor plates were replaced with a pool of LM, such as Ga or Sn. The electrodes, placed inside the pool enable a volumetric Lorentz force to agitate the liquid metal such that the LM temperature at the separatrix strike point can be reduced to the acceptable level.

In spite of significant progress in these and many other studies on implementation of free-surface flows in fusion cooling applications (see, for example a literature review in Ref. 5), many key scientific and engineering issues have not been fully resolved yet, and, as a matter of fact, the practicality of any of the proposed free-surface flow concepts for either the FW or divertor components has not been demonstrated. However, the main difficulties in the implementation of such concepts have been identified and associated studies have progressed. The most serious feasibility issue of all LM free-surface flow concepts is MHD-induced surface instabilities as they may eventually lead to flow disintegration and/or formation of “dry spots” on the solid substrate. Other potential issues associated with the use of LMs are high corrosion rates, plasma-LM interactions and limitations and difficulties in temperature control. As concluded in Ref. 6, “we still cannot state categorically that liquid surface PFCs have the potential for successful development in applications for a CTF or DEMO. But there is general concern about solid wall PFCs for an efficient high temperature fusion reactor. And collective research worldwide on liquid surface PFCs does seem to moving toward a tipping point in the near future. At that point the aggregated evidence will motivate much stronger initiatives for liquid surfaces as a believable approach and an alternate to realizing a robust high power fusion device.”

As such an initiative, the US FESS project team, starting from 2017, examines the application of LMs for PFCs. Our approach has been to utilize an already established fusion design, FESS-FNSF (Ref. 7), including

basic chamber geometry, magnetic configuration and thermal loads, to implement a new technology and develop engineering concepts that utilize free-surface LM flows.

The main purpose of this paper is to report conclusions from extensive LM MHD analysis that shows options for LM FWs and divertors based on the constraints for MHD-controlled LM flows. LM-based FW and divertor concepts also have various other issues, e.g. neutron damage to solid structures, corrosion and mass transfer, and some require electrical insulation, which is challenging in the fusion environment. The design point is a tokamak-based machine with 518 MW fusion power, a 4.8-m major radius, a 1.2-m minor radius and a machine average neutron wall loading ~ 1 MW/m^2 (Fig. 1). A Dual-Coolant Lead-Lithium (DCLL) blanket was already selected as the main breeding blanket concept for this machine, and the MHD thermohydraulic analysis for the lead-lithium (PbLi) flows in the blanket conduits was performed in Ref. 8. In spite of the obvious attractiveness of using the same LM in both the blanket and PFCs, we don't consider PbLi here. Instead, liquid Li was selected as a first candidate to be considered as a working fluid for the liquid FW and for proposed divertor options because of many potential advantages, such as high thermal conductivity and low viscosity, high capability for heat and particle removal and improvements in plasma stability and confinement. In fact, Li-based surfaces are now routinely proposed in numerous magnetically confined fusion devices around the world.[9] However, this Li selection in the present study does not exclude other LM candidates in our future studies for the proposed concepts, including PbLi itself.

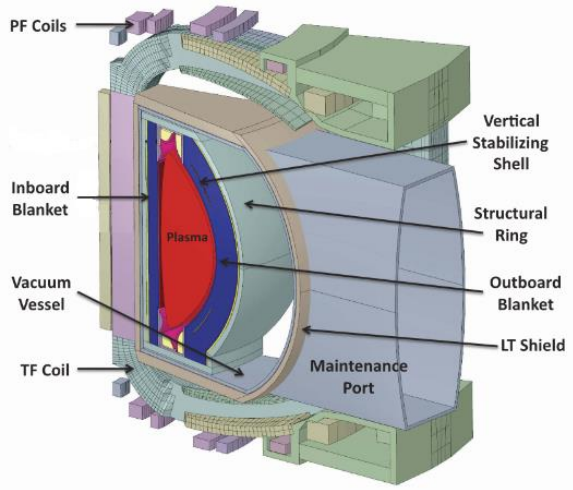

Fig. 1. CAD drawing of one of the 16 sectors of the FESS-FNSF design (courtesy of E. Marriott, University of Wisconsin).

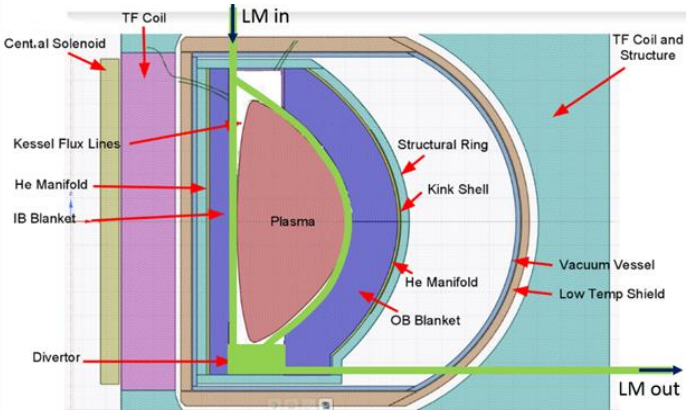

Fig. 2. Schematics of the proposed integrated LM PFC concept, showing the liquid FW in inboard and outboard segments that continues into the open-surface divertor.

With the selection of Li as a working fluid, this paper introduces a new integrated LM PFC concept (Fig. 2) in Section II, including liquid FW and several variants for an integrated open-surface divertor. The two next sections (III and IV) include results and analyses for the flowing Li FW and open-surface divertor correspondingly. Concluding remarks are given in Section V. Descriptions of the mathematical models and computer codes are presented in the Appendix.

II. A CONCEPT AND DESIGN CONSIDERATIONS FOR AN INTEGRATED LM FLOWING FIRST WALL AND OPEN-SURFACE DIVERTOR

The proposed FW design is similar to the CLiFF concept in the APEX study (Ref. 2). Nozzles at the top of the chamber distribute LM on segments of the solid inboard (IB) and outboard (OB) structures. These relatively thin (~2 cm) fast (~10 m/s) layers flow mostly poloidally, towards the bottom of the chamber, and cover the entire FW (Fig. 2).

After removing the surface heat flux (plus some volumetric heat), the LM forms a large area in the divertor with an open surface to absorb the high-peak heat load there. Then the LM moves through one or more drains at the bottom of the chamber to an external system. This includes a pump, a heat exchanger, a purification system and a tritium extraction system (in the case of Li, PbLi or SnLi).

Conditions for the IB and OB differ significantly. The magnetic field over the IB region changes little. The OB magnetic field components (especially the toroidal one) have pronounced variations. Also, the forces on the OB LM flow vary with the poloidal distance due to the poloidal and toroidal curvatures of the solid FW and associated changes in the magnetic field.

Gravity, inertia and centrifugal forces control the adherence of the liquid layer to the OB FW substrate. The concept could also use electromagnetic forces, if needed, to hold the liquid layer against the solid wall. The "magnetic propulsion" proposed in Ref. 10 and analyzed in Ref. 11 for a curved substrate is an example.

A distinctive feature of the proposed PFC concept is that the LM from the FW proceeds to the divertor. A single flow circuit combines all plasma facing components and requires only one set of auxiliary equipment. This is a big engineering advantage compared to other designs with multiple flow circuits.

The main design goal is then to keep the maximum surface temperature of the flowing LM below the limit set by the vapor flux returning to the plasma while the LM is hydrodynamically stable over the entire flow path. This latter requirement does not prohibit small-amplitude surface waves but excludes large flow disturbances on the free surface and in the bulk of the flow. These potentially can destroy the flow or result in formation of dry spots. In contrast, small surface waves may even be useful to increase heat transfer.

For the Li FW, the maximum allowable temperatures in Ref. 12 for a few fusion designs were in the range of 370-480-°C. Using these estimates for our study, we set the maximum allowable surface temperature of Li at 450°C. Since Li melts at ~ 180°C, our choice of 450 °C restricts the design window to about 200 °C.

Several options for the integrated open-surface divertor have been proposed in this paper. The first one is a so-called “tub-like divertor” as sketched in Fig. 3 and also in Fig. 2. Similar to the ACLMD concept in Ref. 4, in the tub divertor, the LM forms a horizontal surface facing the heat flux from the plasma. The distribution of the heat flux over the free surface can be controlled to some degree by changing the location of the liquid level in the tub with respect to the separatrix. In the “deep” divertor (Fig. 3a), the depth of the LM tub is ~ 1 m, while in the “shallow” divertor (Fig. 3b), it is reduced to 0.2-0.5 m. There can be some advantages of the shallow tub compared to the deep tub divertor, including lower Li inventory and better thermal control. Also, the shallow divertor has some flexibility in the vertical positioning of the open surface with respect to the plasma X-point, thus there is more control on the surface heat flux distribution.

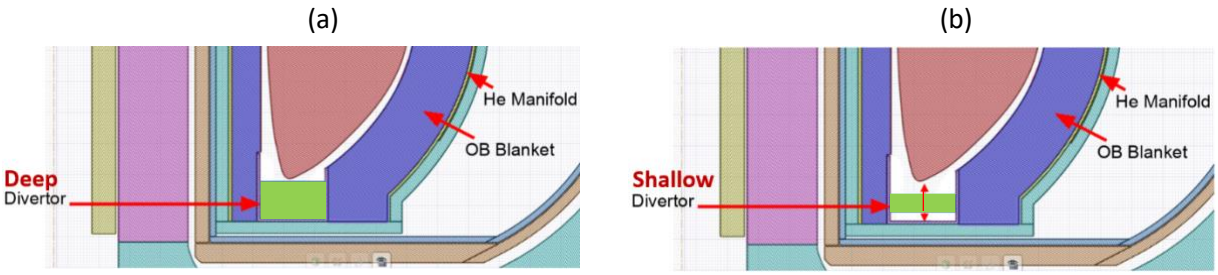

Fig. 3. Schematics for the tub-like divertor concept: (a) "deep" tub, and (b) "shallow" tub. For simplicity, the figure doesn't show the incoming IB and OB streams (shown in Fig. 2).

It should be noted that in spite of some similarity between the newly proposed tub divertor and the earlier ACLMD concept (both have a large horizontal surface), the heat removal scheme in the tub divertor is very different. In our tub divertor design, the absorbed heat energy from the plasma is continuously transported with the flowing LM towards the ancillary equipment through the drain opening/openings at the bottom of the LM pool as shown in Fig. 2. The shape, size, location and also the number of the openings need to be optimized to provide better LM stirring in the pool to possibly minimize the surface temperature. In the ACLMD design, the LM is not circulated and the absorbed thermal energy by the LM is removed with the help of cooling tubes that can be submerged into the LM or placed outside. Such cooling tubes could also be used in the case of the tub divertor to increase its heat transfer capability. Effective thermal stirring in the LM pool is a very important requirement in the present concept as the heat conduction in a stagnant Li pool is a very slow process that would result alone in unacceptably high temperatures on the LM surface. In the tub divertor, the mixing occurs in a natural way by convection caused by two incoming jets from the IB and OB sides and also due to the internal gravity-driven flow from the bulk of the pool towards the drain. If these flows are not sufficient, additional electromagnetic mixing in the LM pool could be provided by injecting electric currents **J**, which in the presence of the plasma-confining magnetic field **B** will be responsible for the agitating Lorentz force **J**x**B**. The cooling tubes, if properly positioned, could be used for heat removal and also as electrodes to inject the electric current at the same time. The Marangoni thermocapillary convection on the free surface is another mechanism that might improve heat transfer in the tub.

Another proposed option for the integrated open-surface divertor is a "fast flow divertor" as shown in Fig. 4, which utilizes the more traditional approach using divertor plates to guide the flow at some angle with respect to the horizon. Figure 4a shows a "three-leg divertor" design in which the inner and outer leg flows originate from the incoming IB and OB streams on the solid FW. There is a middle leg between the inner and outer divertor legs. The liquid is drained at the lowest point of the middle leg where the flows from the middle leg and the outer leg merge. Such a divertor geometry is a rough approximation for the curvilinear-plate divertor (Ref. 13) using three flat-plate segments. To assure more or less smooth flow transition from the liquid wall to the divertor, the flows coming from the FW are redirected using two deflectors (as in Ref. 3) as also shown in Fig. 4a. Figure 4b shows a "two-leg divertor", which is a further simplification of the three-leg divertor. In what follows in this paper, we limit our analysis of the fast flow divertor to the two-leg design.

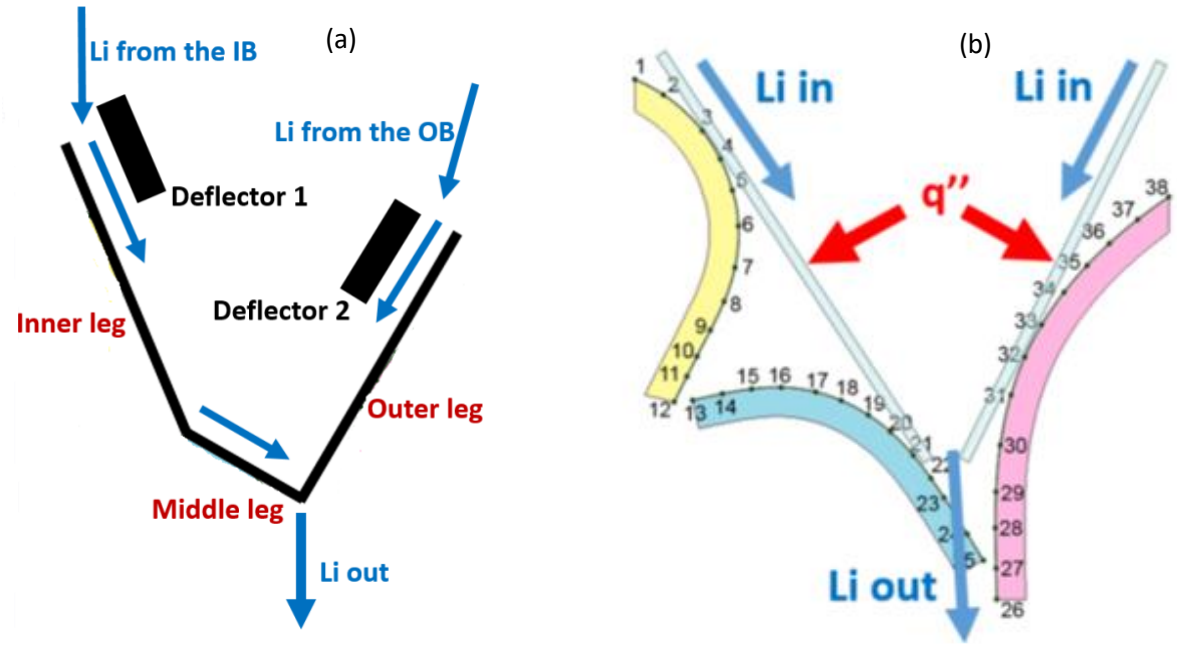

Fig. 4. Schematics for the fast flow divertor concept: (a) "three-leg divertor", and (b) its simplified version "two-leg divertor".

An important design decision is whether or not the liquid FW and the LM flows in the divertor region at the bottom of the reactor chamber are subdivided toroidally into separated sectors reproducing the modular structure of the FESS-FNSF design with the 16 sectors as shown in Fig. 1. In fact, the DCLL blanket behind the solid FW was designed in such a way.[8] A LM PFC design without breaking the flow into sectors such that the liquid wall and the divertor flow are continuous in the toroidal direction (axisymmetric design) seems to be the simplest. However, there are two groups of arguments in favor of the sector design. From the engineering viewpoint, a sector design (such that the LM flow in each sector is completely separated from other sectors) might be necessary to avoid LM leaking through the gaps in the solid FW. On the other hand, insulating dividing walls might be needed to break toroidal currents caused by a radial magnetic field component, which, even being small, may lead to strong flow-opposing Lorentz forces. Looking ahead, it should be noted that our MHD analysis in Section III shows that the dividers are needed to avoid flow stopping by strong electromagnetic forces in some parts of the OB segment, where the radial magnetic field component is higher than ~ 0.05 T. Based on these two arguments, in what follows, we will focus on a sector design of 16 sectors, assuming that the LM flow in each sector (both in the liquid FW and divertor) is completely separated using the dividers that stretch poloidally all the way down from the chamber top to the bottom. To serve as insulating breakers, the dividers need to be made electrically non-conducting, for instance, of silicon carbide or alumina.

III. RESULTS AND ANALYSIS FOR THE FLOWING Li FW

III.A. Characterization of the Flowing Li FW in the IB and OB Regions

Table I shows major parameters, which were used as an input data in the present analysis of the liquid wall. Some parameters are, in fact, not constant and experience variations along the LM flow path. Such parameters are indicated in the first column of the table with an asterisk (*). Although not shown in the table, these variations were incorporated in the computations such that the computed results do include effects of spatial changes in the magnetic field, radius of curvature and toroidal width. Two flow parameters, the inlet velocity U_0 and the inlet flow thickness h_0, are subject to optimization. Some results from the optimization studies are shown below, in this section.

Table I. Characteristic parameters in the Li FW flow at the FNSF inboard and outboard

Parameter	FW, Outboard	FW, Inboard
Toroidal B-field, B_{tor}*	6 T	10 T
Radial B-field, B_{rad} *	0.5 T (maximum)	0.05 T (maximum)
Surface heat flux, q'' *	0.24 MW/m^2	0.16 MW/m^2
Volumetric heat flux, q''' *	8.5 MW/m^3	6.2 MW/m^3
Inlet temperature	350°C	350°C
Flow length, L	10 m	7 m
Radius of poloidal curvature *	10.7 m (top) 1.9 m (mid-plane)	∞
Toroidal width, $2b$ *	2.3 m	1.7 m

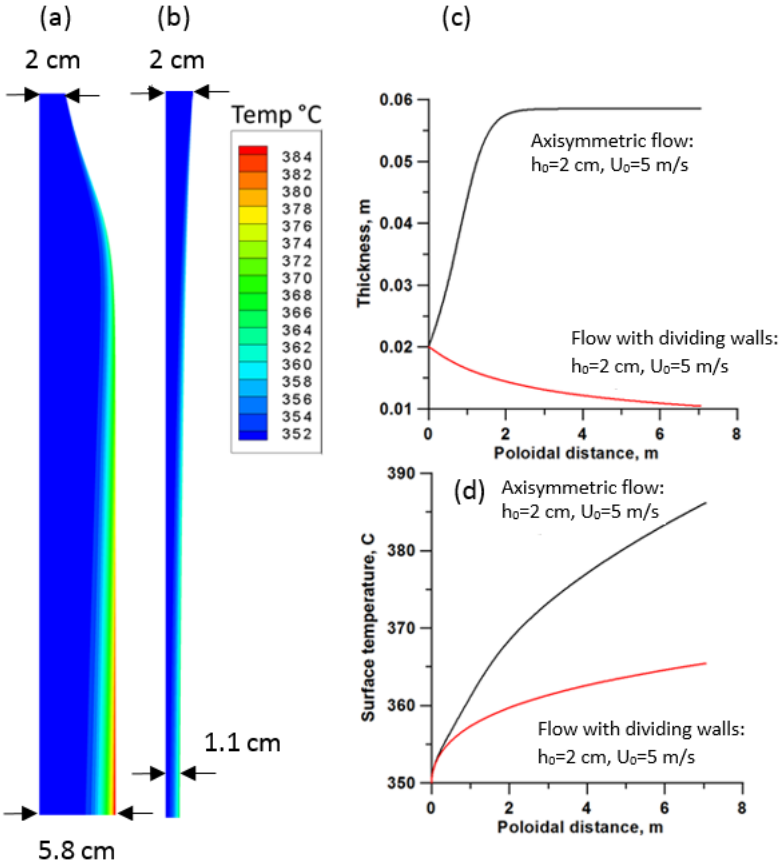

Fig. 5. IB region. Computed Li FW flow thickness and temperature distribution at h_0=2 cm and U_0=5 m/s:

(a) Axisymmetric flow,
(b) Flow with dividers,
(c) Comparison of the flow thickness,
(d) Comparison of the surface temperature.

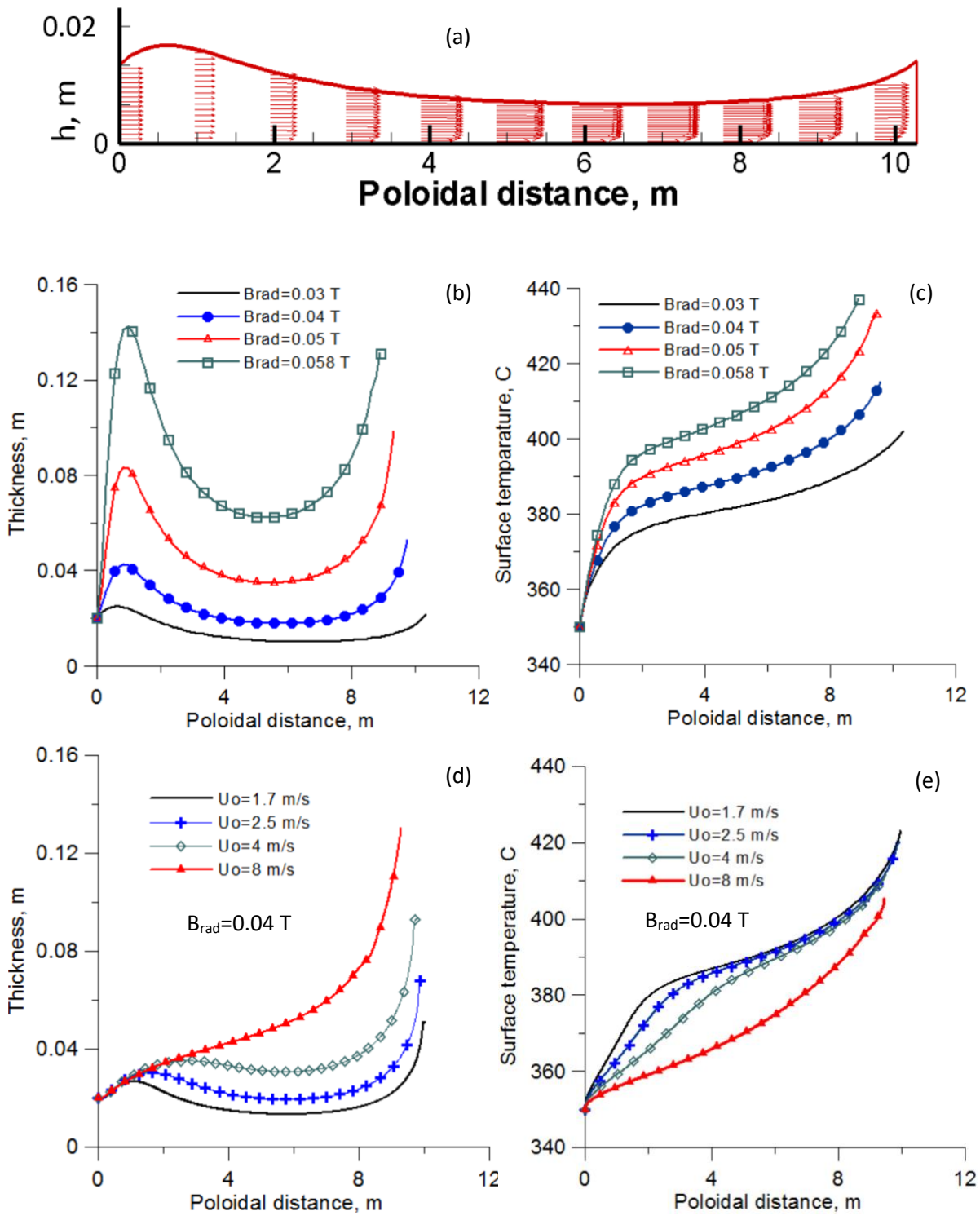

Fig. 6. OB region. Axisymmetric flow. Computed Li FW and temperature distribution at h_0=2 cm: (a) Flow thickness and velocity distribution at U_0=2 m/s and B_{rad}=0.03 T, (b) and (c) Effect of the radial magnetic field B_{rad} at U_0=2 m/s, and (d) and (e) Effect of the velocity at B_{rad}=0.04 T.

Figure 5 shows typical results computed for the IB region for axisymmetric flows and flows with the dividing walls (sector design). Figure 6 illustrates results for axisymmetric flows in the OB region and Fig. 7 for the case when the dividing walls are present. The temperature distributions in Figs. 6c and 6e suggest a very strong effect of the inlet flow velocity and the radial magnetic field on the temperature field. This effect is related to the poloidal variations in the liquid layer thickness and velocity. Significant increase in the surface temperature near the bottom of the reactor chamber can be explained by the layer thickening and associated velocity decrease. In the axisymmetric design, the most critical magnetic field component is the radial one, while the toroidal field almost doesn't affect the flow. Even small, the radial field component can cause significant flow thickening. In the inboard region, B_{rad} is only 0.05 T but such a field may cause tripling of the flow thickness as shown in Fig. 5. The most dramatic effect of B_{rad} was however observed on the OB flow. Here, the maximum B_{rad} is 0.5 T but even much lower B_{rad} may result in a kind of hydraulic jump in the lower section of the flow as shown in Fig. 6b and Fig. 6d. Because of this reason, it has been decided to abandon the axisymmetric design in favor of the flow design with the dividing walls. In such a sector design, the flow opposing Lorentz force arises from the cross-sectional currents in each sector attributed to the toroidal field component, but the flow variations along the poloidal path are still much smaller compared to the axisymmetric design as seen in Fig. 7.

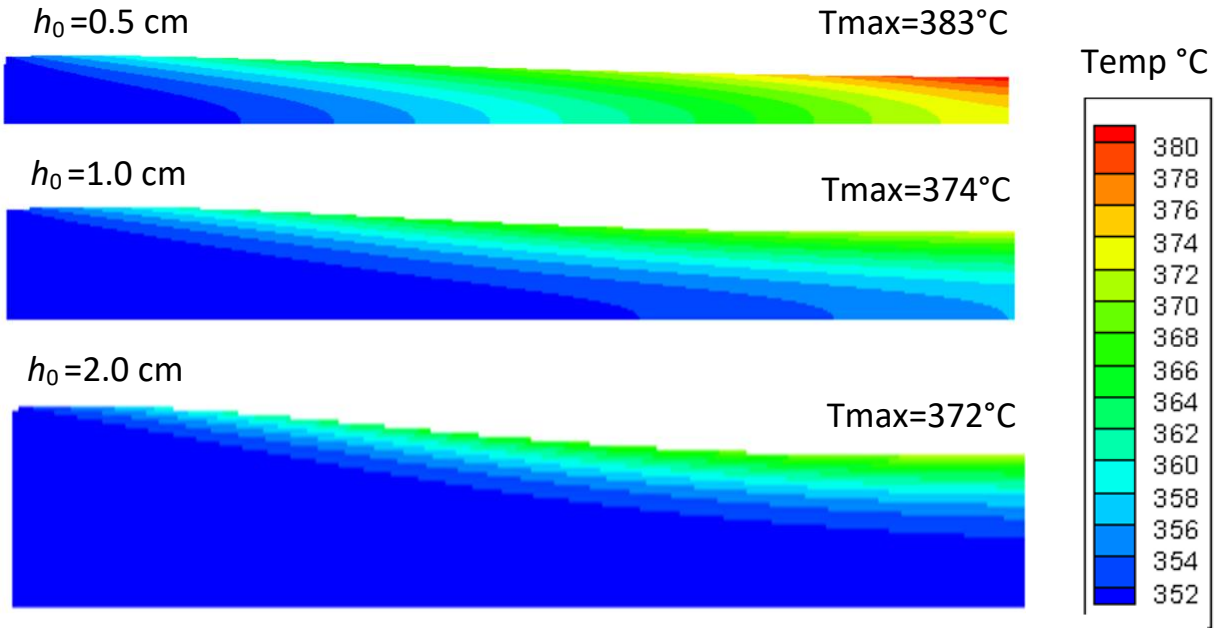

Fig. 7. OB region. Flow with the dividers. Effect of the inlet flow thickness on the flow development and temperature distribution at U_0=10 m/s and B_{tor}=10 T.

III.B. Maximum Surface Heat Flux

Special analysis was performed to evaluate a maximum surface heat flux that can be removed by the flowing Li FW. It should be noted that the surface heat flux on the FW under the FNSF conditions is not high as shown in Table I and, as a matter of fact, can be easily removed by turbulent helium flows at a relatively low heat transfer coefficient in He gas of ~ 2000 W/m^{2}K, providing RAFM steel (reduced activation ferritic-martensitic steel) is used as a structural material. We use, nevertheless, the reference FNSF design as a testing environment in our evaluations of the maximum heat flux by increasing q'' to

significantly higher values until the maximum surface temperature T_{max} becomes higher than the maximum allowable one, i.e. 450°C for Li. Results are shown in Figs. 8, 9 and 10 for the flow with dividers.

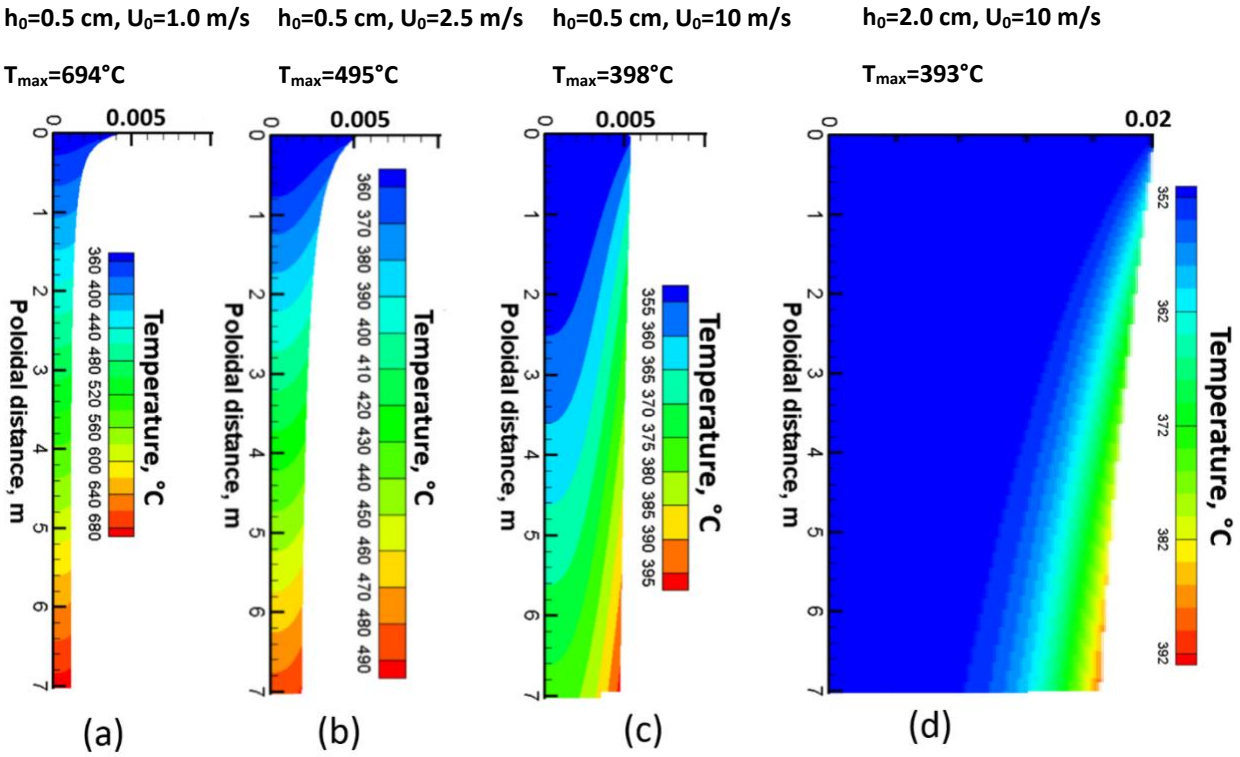

Fig. 8. Computed temperature distributions in the flowing Li FW for different h_0 and U_0 at q''=0.5 MW/m^2 (IB region, flow with dividers): (a) h_0=0.5 cm, U_0=1 m/s resulting in T_{max}=694°C, (b) h_0=0.5 cm, U_0=2.5 m/s resulting in T_{max}=495°C, (c) h_0=0.5 cm, U_0=10 m/s resulting in T_{max}=398°C, (d) h_0=2.0 cm, U_0=10 m/s resulting in T_{max}=393°C.

Figure 8 shows several temperature fields computed for the surface heat flux of 0.5 MW/m^2, which is more than three times higher than that in Table I. Of three velocities used in the analysis, two of them, 1 m/s and 2.5 m/s result in high surface temperature that exceeds 450°C while the velocity of 10 m/s results in a surface temperature lower than 400°C for two flow thicknesses 0.5 cm and 2 cm. In the next analysis shown in Fig. 9, we fixed the flow thickness at 2 cm and the inlet velocity at 10 m/s and increased incrementally the surface heat flux from 0.5 MW/m^2 to 2 MW/m^2. The analysis shows that at these flow parameters the maximum surface heat flux that can be tolerated by the flowing Li layer can be higher than 1 MW/m^2. An example of the fine tuning of the flow parameters is shown in Fig. 10, where T_{max} of 450°C was achieved at U_0=7 m/s, h_o=2 cm and q''=1.1 MW/m^2. Obviously, higher heat fluxes, more than 1 MW/m^2, might also be acceptable but this will require very high flow velocities, more than 10 m/s. In practice, establishing stable FW flows at such high velocities might be challenging.

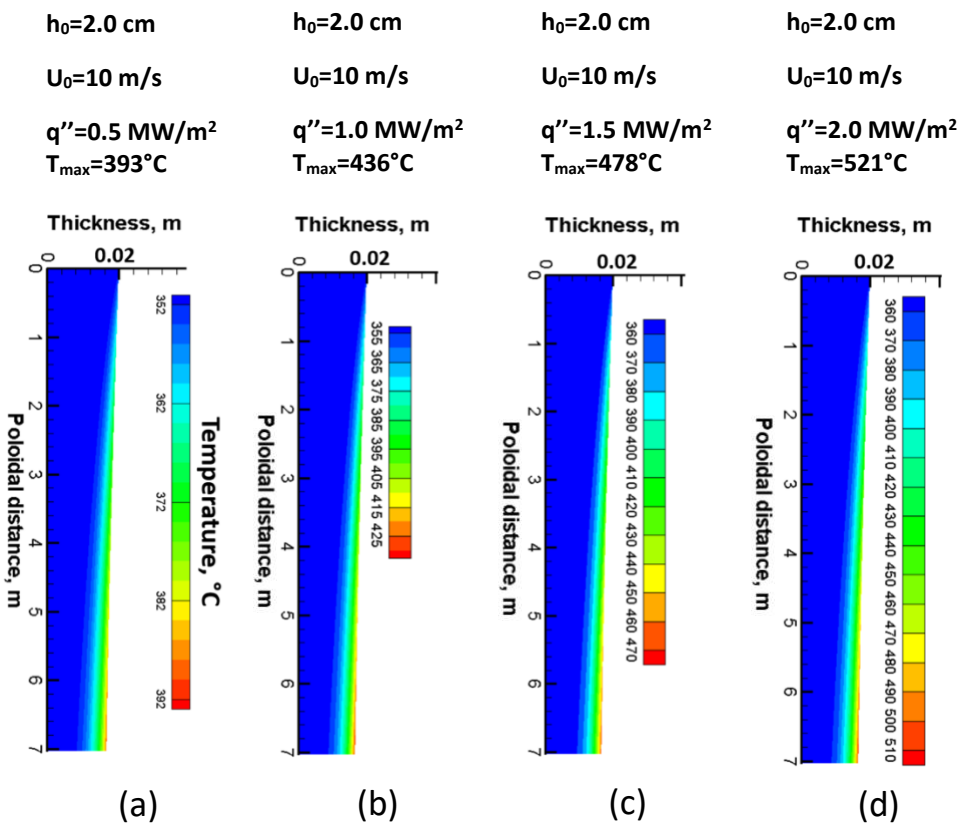

Fig. 9. Effect of increasing q'' on the temperature distribution in the flowing Li FW at h_0=2 cm and U_0=10 m/s (IB region, flow with dividers): (a) q''=0.5 MW/m^2 resulting in T_{max}=393°C, (b) q''=1.0 MW/m^2 resulting in T_{max}=436°C, (c) q''=1.5 MW/m^2 resulting in T_{max}=478°C, (d) q''=2.0 MW/m^2 resulting in T_{max}=521°C.

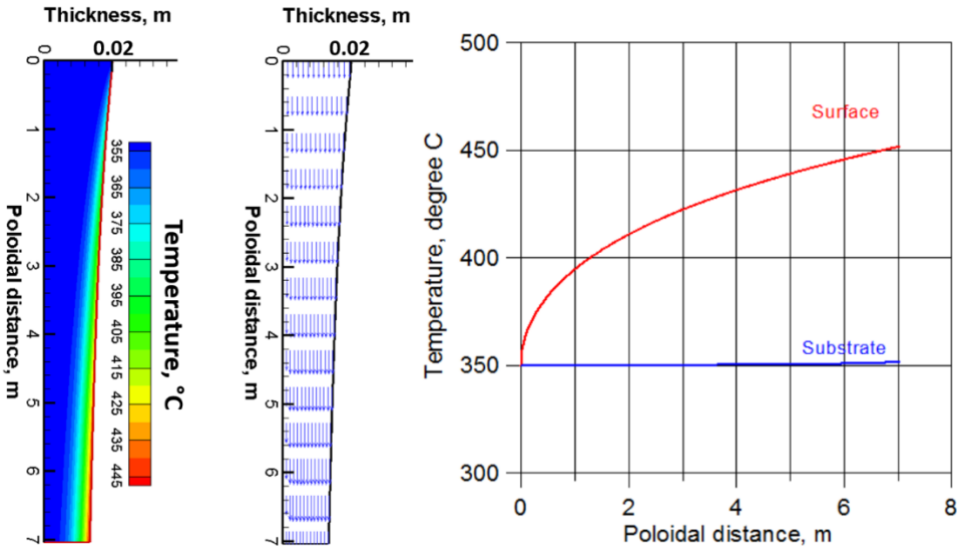

Fig. 10. Example of the Li FW (IB region, flow with dividers) with T_{max}=450°C at h_0=2 cm, U_0=7 m/s and the applied surface heat flux q''=1.1 MW/m^2.

III.C. Optimization Studies

We have proposed several design criteria/requirements on the flowing LM FW, such as:

1. The LM layer needs to be adhered to the solid substrate and remain stable - Mandatory,
2. Maximum temperature on the free surface has to be lower than the maximum allowable temperature (450°C for Li as adopted in this study) to limit the vapor flux into plasma - Mandatory,
3. Substrate temperature has to be lower than the maximum allowable temperature defined by the material limits (550° for RAFM) - Mandatory,
4. The flow thickness should be almost uniform over the entire poloidal flow path,
5. To reduce the pumping power, the flow rate in the FW needs to be as low as possible,
6. Liquid metal removes all the surface heat flux,
7. Flow rate in the flowing LM FW is high enough to agitate liquid in the divertor pool for better heat transfer.

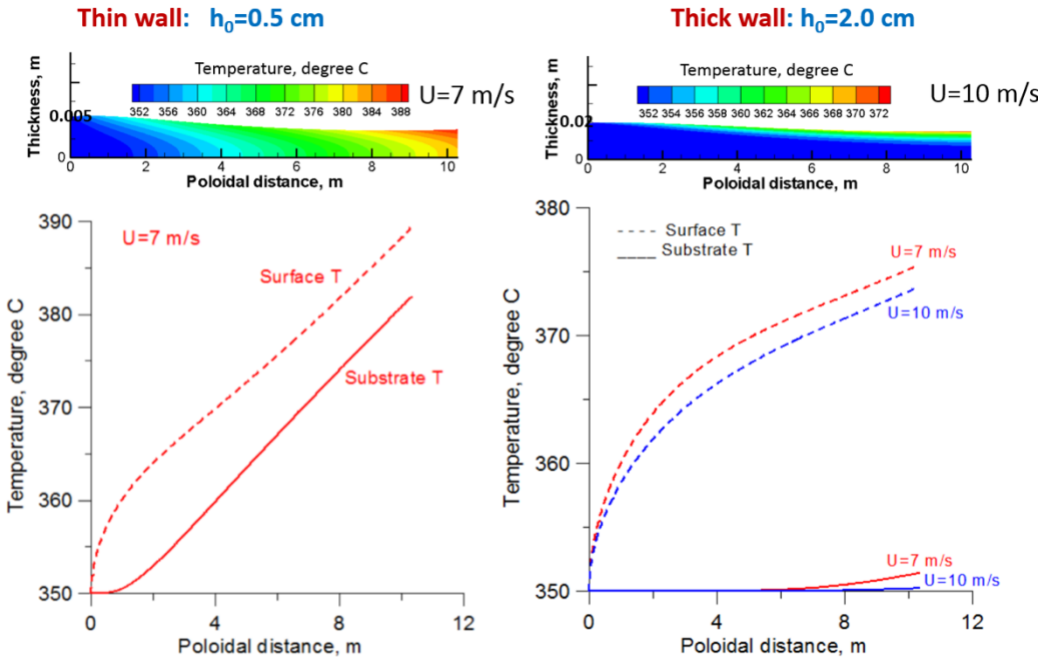

Fig. 11. Examples of thermally "thin" (left) and "thick" (right) Li FW. Computed for the OB region for the sector design with dividing walls.

The optimal liquid FW design should satisfy all the proposed criteria, but in practice not all of them need to be met. Some of them, such as 1, 2 and 3 are mandatory; others have a lower priority. In fact, all the requirements cannot be equally satisfied at the same time. Namely, requirements 1, 2, 3, 4, 6 and 7 suggest higher flow velocities, while requirement 5 on minimization of the pumping power suggests the opposite. Therefore, one needs to look for a tradeoff. Based on the proposed criteria, in what follows, we will distinguish between two possible FW options: thermally "thin" and "thick" LM walls. The differences between them can be seen in Fig. 11, which shows temperature distributions in the Li FW flow for two IB flows at h_0=0.5 cm (thin) and h_0=2 cm (thick). The thick wall (Fig. 11, right) removes all the surface heat

flux such that the heated area is localized near the free surface, while the surface temperature remains below the maximum allowable temperature of 450°C. In the case of the thin wall (Fig. 11, left), the surface temperature is also below 450°C but the heat flux from the free surface penetrates across the entire thickness down to the solid substrate. If so, only a portion of the surface heat flux will be removed by the flowing LM. Obviously, the thin wall is acceptable from the design point of view as long as both requirements 2 and 3 are met. In the case of Li FW and RAFM structure, requirement 3 is automatically satisfied providing requirement 2 is met. This, however, might not be the case if another LM (rather than Li) with higher maximum allowable temperature (for example, Sn) is used.

Requirement 1 matters only for the OB, where the flow is retained against the solid substrate by the joint action of gravity, centrifugal and electromagnetic forces. While the centrifugal force is always directed to the solid substrate, the gravity and electromagnetic forces can change their direction as the liquid moves downstream. Our estimates suggest that the OB flow has to be at least 7 m/s to make sure that the liquid remains on the wall. The most critical section of the flow is that at the top of the chamber where the outward gravity force component is maximal. As demonstrated in Fig. 11, the OB FW at h_0=2 cm and U_0=7-10 m/s does its job, removing all surface heat flux and keeping the maximum temperature at the free surface well below 450°C. In the IB region, high velocities are not needed. In fact, our analysis shows that the thin IB layer at h_0=0.5 cm has the surface temperature lower than 450°C providing U_0 is as low as 1.1 m/s. To conclude, based on the present analysis, which is limited to the thin-shear-layer approximation, the design window for the Li FW in both the IB and OB regions is sufficiently large, especially for the IB.

IV. RESULTS AND ANALYSIS FOR THE PROPOSED DIVERTOR DESIGNS

Major parameters, which we used in the analyses for the proposed divertor options, the tub divertor and the fast flow divertor, are summarized in Table II.

Table II. Characteristic parameters used in the analyses for the proposed Li divertor designs

Parameter	**Tub-like divertor**	**Two-leg fast flow divertor**
Surface heat flux *q''*	Model bell-type profile with the base ~ 5-cm and the peak at 10 MW/m^2	Model bell-type profile with the base ~ 5-cm and the peak at 10 MW/m^2
Dimensions	Deep tub: *Vertical* = 1 m *Horizontal (radial)* = 1 m *Horizontal (toroidal)* = 1.5 m Shallow tub: V*ertical* = 0.2 m *Horizontal* (radial) = 1 m *Horizontal* (toroidal) = 1.5 m	Inner leg: *Length* = 1.02 m *Inclination angle* = 54° Outer leg: *Length* = 0.86 m *Inclination angle* = 64°
Magnetic field	Only toroidal: B_{tor} = 7 T	Only toroidal, B_{tor} = 7 T

Results of the analysis are shown below in sections IV.A, IV.B and IV.C. It should be noted that because of several reasons the present computations don't have the Marangoni effect and buoyancy-driven flows. As for the buoyancy-driven flows, the buoyancy forces and associated flow effects are not expected to be strong because the heat flux is applied from the top. The Marangoni effect at q'' ~ 10 MW/m^2 might be

strong but was not included either because of significant computational challenges and associated long computational time due to coupling between the velocity and temperature field as seen from Eq. (9). The estimates in Ref. 24 that used experimental data for a high-power e-beam at 60 MW/m^2 predict the velocity of the liquid Li surface in the presence of high temperature gradients at 10 m/s. In this study, only a few computations were performed with the Marangoni effect in the presence of a magnetic field to test the code. These tests included two relatively low heat fluxes of 700 and 3500 W/m^2 at B_{tor}=0.5 T. A five-time increase in q'' resulted in about two-time increase in the themocapillary convection speed from ~0.5 mm/s at q''=700 W/m^2 to ~ 1 mm/s at q''=3500 MW/m^2.

IV.A. Heat Transfer Mechanisms in the Li Pool

Although all liquid metals, Li in particular, are good thermal conductors, heat diffusion by itself is not sufficient to keep surface temperature in the tub-like divertor low enough. A time evolution of the temperature field in a stagnant pool of Li, heated from the free surface using high-peak surface heat flux at 10 MW/m^2 was computed to estimate the speed of heat propagation into stagnant Li. The temperature front spreads slowly into the Li bulk reaching the bottom wall, which in this computation was placed at a distance of 20 cm from the free surface, in about 400 s. If so, the speed of the heat diffusion process in the Li is roughly 0.5 mm/s. This is a very slow transport process compared to the convection of heat, which in the presence of the incoming jets from the IB and OB and internal gravity-driven flows occurs at several m/s. Also, the maximum temperature at the free surface at 400 s is unacceptably high ~ 8500°C.

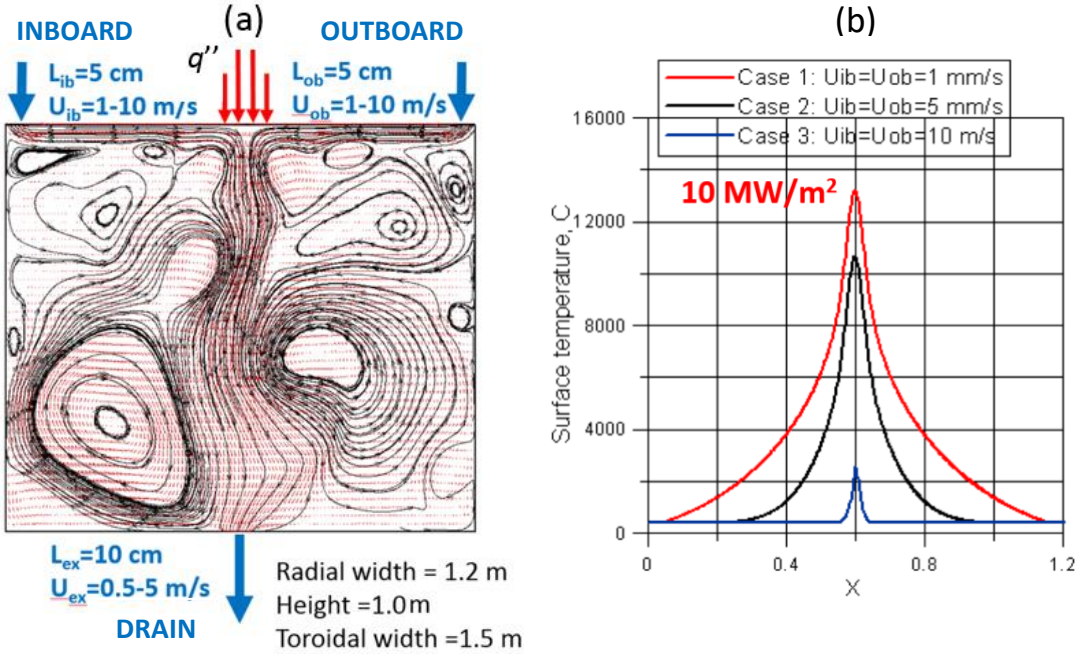

Fig. 12. The analysis of heat transfer mechanisms in a LM tub-like divertor: (a) sketch of the Li "deep" pool showing location of the incoming IB and OB jets, drain orifice, applied heat flux and the flow field in the liquid, and (b) computed time-averaged surface temperature at three different IB/OB jet velocities: 1 mm/s, 5 mm/s and 10 m/s.

We have identified a few convective heat transport mechanisms for the tub-like divertor, using a deep tub as an example. In this example (Fig. 12), two velocity streams from the IB and OB hit the surface of the deep Li pool, creating a special flow distribution in the pool. Besides the jets, the flow inside the pool is strongly affected by the position and size of the drain orifice, which is located at the bottom of the pool at the center. The flow velocity through the drain and the drain width are denoted U_{ex} and L_{ex}. In fact, there might be as many orifices as needed to provide a flow pattern that might result in a more intensive heat transfer, but in our first analysis there is only one with L_{ex}=10 cm. The incoming jet velocities U_{ib} (at the IB) and U_{ob} (at the OB) and corresponding jet widths L_{ib} and L_{ob} are used as parameters. These parameters are shown in Table III.

Table III. Parameters in the six computed cases to characterize convection in the Li pool

Case #	B, T	Uib	Uob	Ma	Time, s Comp/Fill	Heat transfer mode
1	7	1 mm/s	1 mm/s	0	26104/12480	Diffusion
2	7	5 mm/s	5 mm/s	0	5221/2496	Diffusion + laminar convection
3	7	0.5 m/s	0.5 m/s	0	52.2/25	Laminar convection + diffusion
4	7	4 m/s	4 m/s	0	6.53/3	Q2D turbulent convection
5	7	10 m/s	10 m/s	0	2.61/1.3	Q2D strong turbulent convection
6	7	1 m/s	5 m/s	0	8.7/4.2	Q2D turbulent convection, asymmetric

The velocities U_{ib} and U_{ob} are not necessarily the same. In fact, Case 6 shown in the table has U_{ob} five times higher than U_{ib} resulting in a strongly asymmetric flow. In the other five cases, the two jets are identical but the flow can still demonstrate significant asymmetries once it becomes turbulent. The fifth column in the table shows the Marangoni number *Ma* (the measure of the Marangoni effect), which in the present analysis was zero, indicating that no Marangoni convection was included. The sixth column shows the computational time versus the time needed to fill the pool. The ratio of these two times in all computations, as seen from the table, is around two to make sure that the computational time is large enough to reach statistically steady-state flow. Figure 13 shows instantaneous flow patterns computed at six different jet velocities from very low at 1 mm/s to very high at 10 m/s. When the jet velocity is increased, the flow regime in the tub changes from the laminar diffusion case (Case 1) to a strong turbulent flow (Case 5). The overall goal of the analysis is to find an optimal combination of the parameters that results in a more intensive heat transport from the surface to the bulk of the domain and eventually outside. At low velocities (Cases 1-3), the flow is fully symmetric and hydrodynamically stable, while at higher velocities (Cases 4-6) it is unstable and even turbulent. After hitting the free surface the two incoming jets turn to flow tangentially to the free surface forming two opposing near-surface jets. At the middle of the pool, where the heat flux is applied, the two horizontal streams collide making a vertical jet (see Cases 3-5). Obviously, the dominant heat transfer mechanism is due to convection by transporting the heat flux from the surface with the vertical jet to the central part of the pool and eventually outside through the drain orifice. An additional heat transfer mechanism, also by convection, is due to turbulent vortices, which can be seen in a big number in the bulk flow as a result of interaction of the horizontal jets

and the central vertical jet with the bulk liquid. These vortices can provide good thermal mixing resulting eventually in a lower temperature at the free surface.

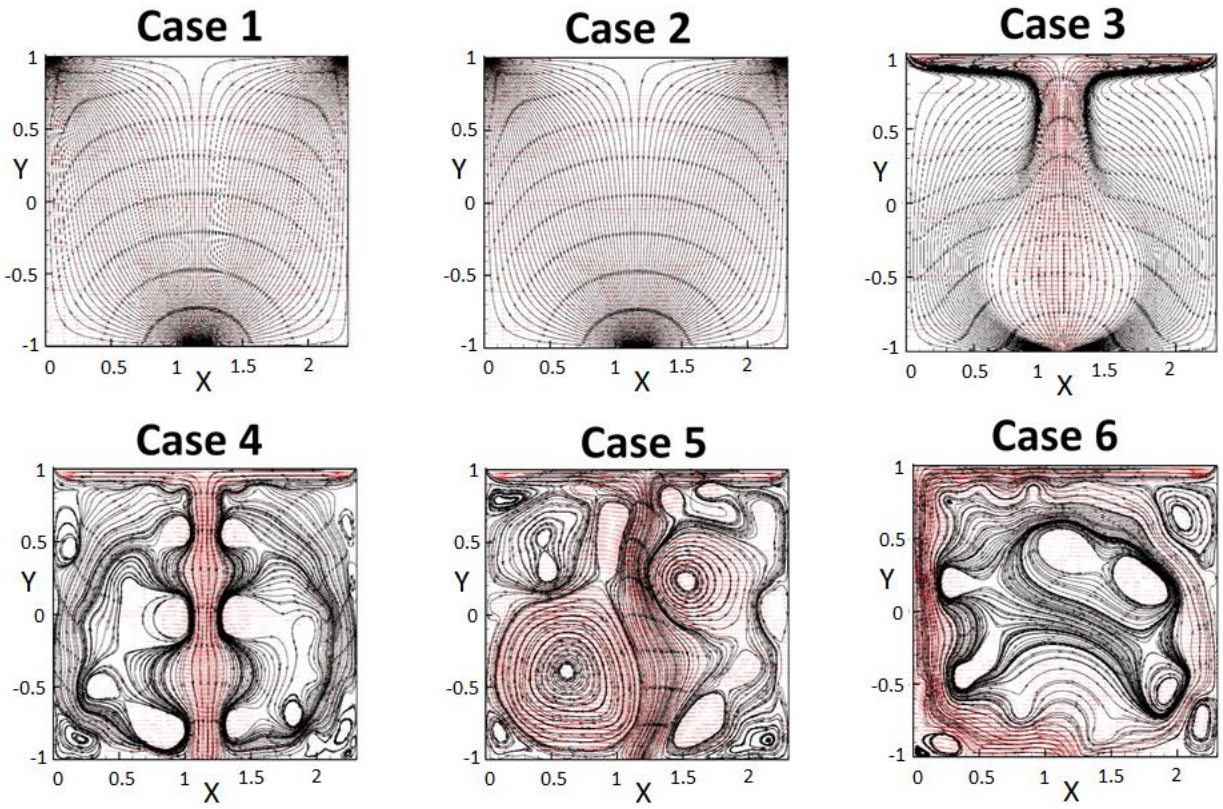

Fig. 13. Instantaneous convective flow patterns in the Li tub (for parameters, see Table III). The figure shows flow streamtracers and velocity arrows. The locations of the IB and OB streams and the drain are the same as in Fig. 12.

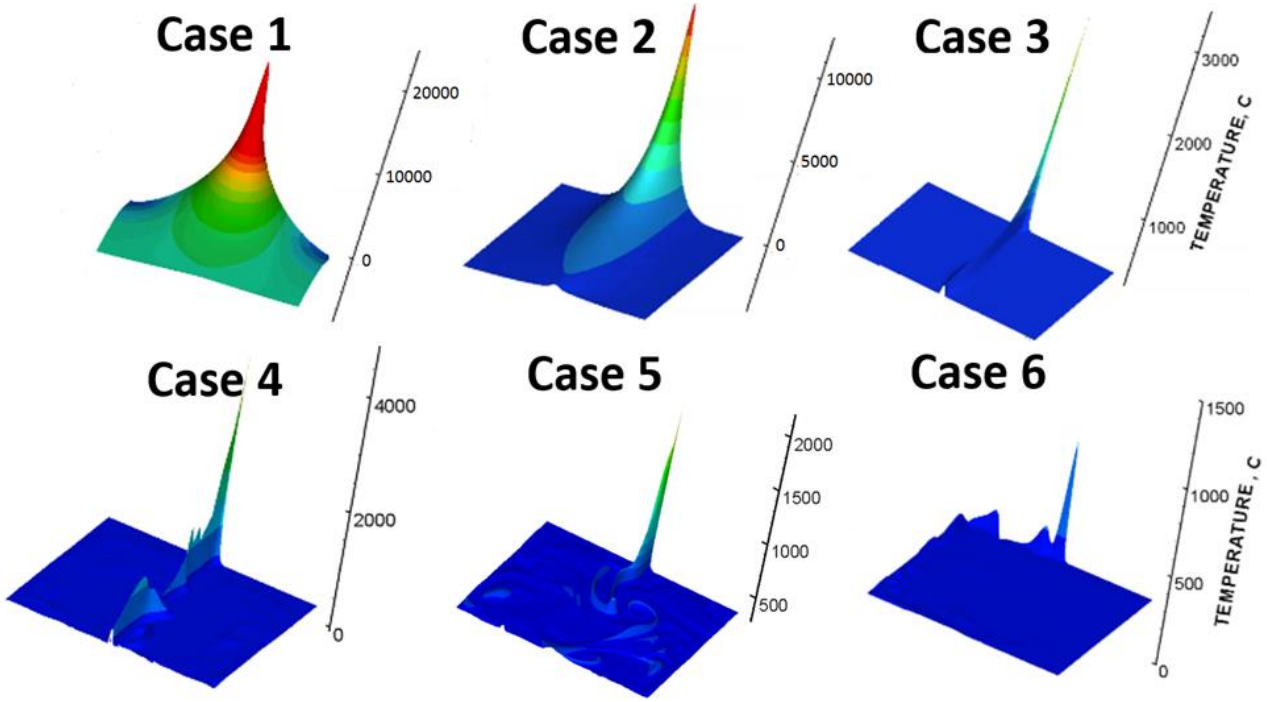

Fig. 14. Instantaneous temperature distributions in the Li pool computed for the six cases specified in Table III.

Such velocity distributions have a direct impact on the temperature field as seen in Fig. 14. Obviously, higher incoming jet velocities allow for a lower temperature on the free surface. However, the strongest temperature reduction to about 1000°C was observed in asymmetric Case 6, where the velocities U_{in}=1 m/s and U_{ob}=5 m/s are significantly lower than the corresponding jet velocities in symmetric Case 5, where U_{ob} and U_{ib} are 10 m/s while the maximum temperature at the free surface is around 2000°C. Based on this comparison, one can conclude that the heat transfer mechanism associated with the near-surface horizontal jet is significantly stronger than that due to the vertical flow. A practical recommendation is therefore to make sure that either the drain orifice is shifted horizontally from the location of the maximum heat flux on the free surface or the velocities of the two incoming jets are significantly different. If so, the horizontal near-surface jet would first be responsible for spreading the heat flux over the free surface more uniformly and then the vertical gravity-driven flow will further transport the thermal energy from the surface towards the drain. This mechanism is further illustrated by the example of a shallow tub-like divertor, where even better reduction of the temperature at the free surface was demonstrated.

IV.B. Results and Analysis for the Shallow Divertor

In the case of the shallow tub-like divertor with the pool depth of 20 cm, two different locations of the drain orifice were considered, while other parameters were the same as shown in Fig. 15.

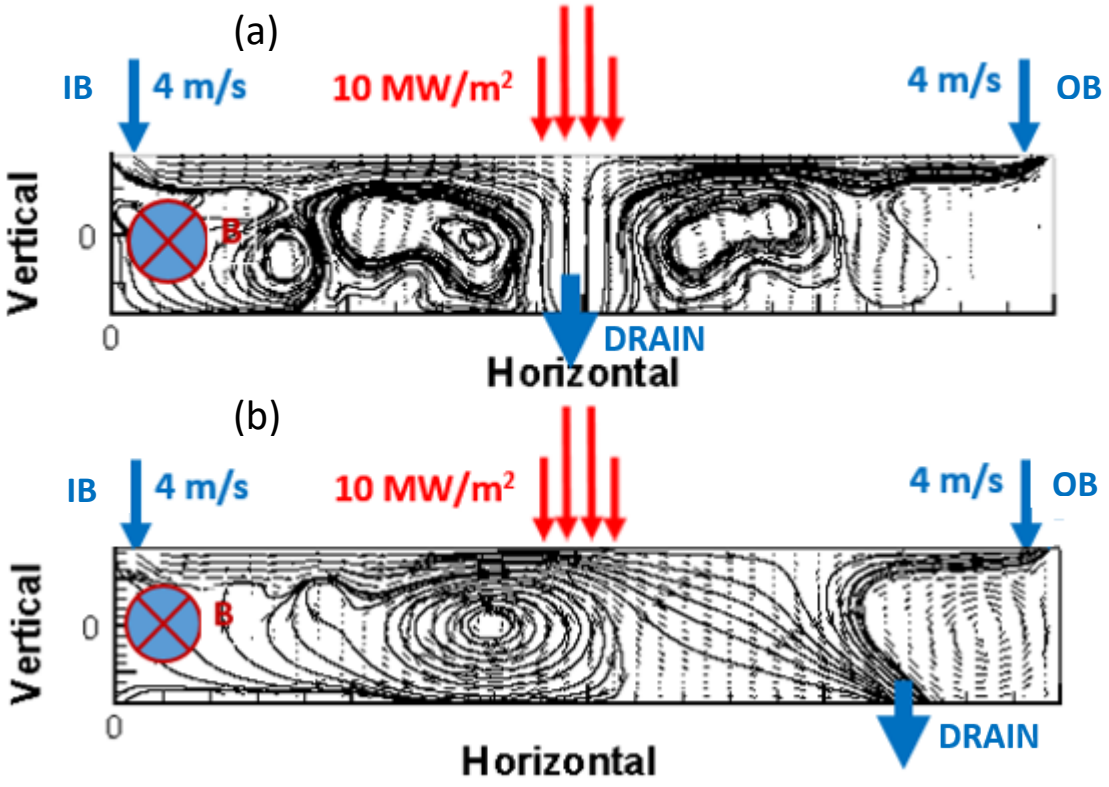

Fig. 15. MHD/heat transfer analysis for the shallow tub-like divertor. The figure shows the locations of the incoming IB and OB jets, drain orifice, applied heat flux and the computed flow field in the liquid for two configurations: (a) the drain is at the middle of the pool, and (b) shifted in the radially outward direction to x=1 m.

Figure 15a shows a divertor configuration where both the heat flux and the drain have the same horizontal location, at the middle of the pool. In such a configuration the surface heat flux is immediately convected by the vertical jet towards the bottom of the pool. The maximum time-averaged temperature at the free surface was found at ~ 1200°C as seen in Fig. 16. Figure 15b shows another configuration where the drain was shifted from the middle of the pool radially outward to x=1 m. In such a case, the flow pattern is different and the temperature distribution at the free surface is also very different (Fig. 16). An important conclusion is that such a combination of the two flows, horizontal and vertical, results in a significantly lower maximum temperature at the free surface of about 450°C. This example clearly demonstrates that the shallow Li divertor does its job by providing the maximum surface temperature to be lower than the maximum allowable temperature.

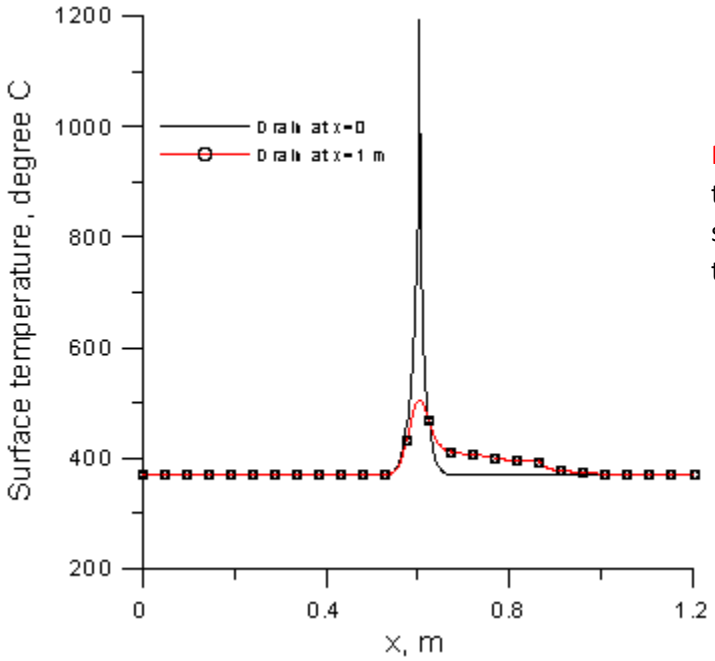

Fig. 16. Computed time-averaged temperature distribution at the free surface of the shallow tub-like divertor for two drain locations shown in Fig. 15.

IV.C. Results and Analysis for the Two-leg Fast Flow Divertor

A sketch of the two-leg fast flow divertor is shown in Fig.4b, the design is described in Section II, and the parameters are given in Table II. The computed flow thickness and the free surface temperature distributions for the inner and outer legs are shown in Fig. 17. Both inner- and outer-leg flows demonstrate only small variations in the layer thickness over the ~ 1-m flow path (Fig. 17a) because of a strong flow inertia associated with the high inlet flow velocity at 10 m/s. Near the inlet, the flow thickness slightly increases and then monotonically decreases due to the gravity effect. The temperature at the free surface demonstrates a high peak at the heat flux hit point and then gradually decreases downstream. In doing so, the maximum Li surface temperature is smaller than 440°C. This is the most important conclusion from the analysis as the fast flow divertor, similar to the shallow tub-like divertor, does provide the maximum surface temperature below 450°C.

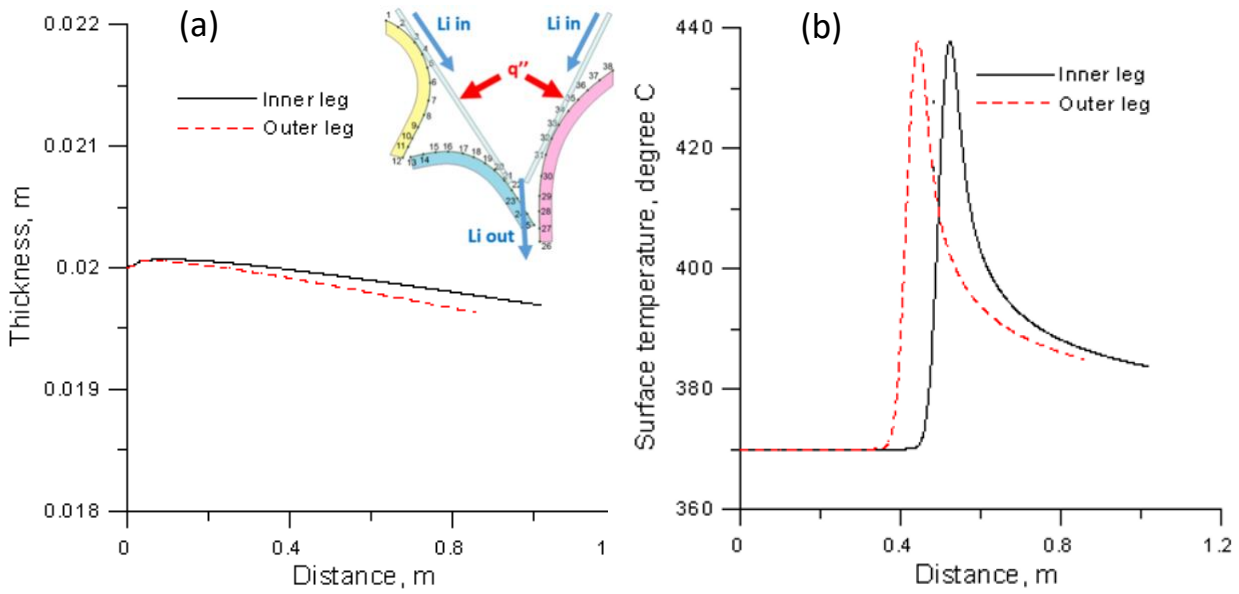

Fig. 17. Results of the MHD/heat transfer analysis for the two-leg fast flow divertor: (a) flow thickness versus distance, and (b) Li temperature at the free surface. For parameters, see Table II.

V. CONCLUDING REMARKS

In this study we proposed a concept of integrated LM PFC, including a liquid flowing FW and an open-surface divertor. In our analysis we used liquid Li as a working fluid and the US Fusion Nuclear Science Facility as a reference fusion reactor design. The MHD flows and heat transfer were analyzed using simplified 2-D models, which to a large degree capture the most important flow features associated with the presence of a free surface, effect of a magnetic field, curved geometry of the substrate, and volumetric and surface heating. These models can be considered as a "first approximation" compared to "zero approximation" models that typically utilize 1-D transport-type equations and available analytical solutions. With the help of these models we were able to demonstrate, in general, the feasibility of the proposed concept. The flowing Li layer on the solid FW remains adhered to the curved substrate, providing the flow velocity is higher than about 7 m/s. The flowing Li FW (at U_0~10 m/s and h_0~2 cm) is capable of removing surface heat flux of ~ 1 MW/m^2 while keeping the free surface temperature below the maximum allowable temperature. Of the several proposed divertor options, the two-leg fast flow divertor has the best heat removal capability. The shallow tub-like divertor was also demonstrated to remove a high-peak surface heat flux of 10 MW/m^2. However, in spite of these positive conclusions, one should keep in mind that the models used have a limited range of applicability and thus cannot predict some special flow features that may also be important and under certain circumstances, even critical to the design. First, the wavy interface, possible droplet and bare spot formation as well as flow detachment from the solid substrate cannot be fully predicted with the present models because of their limitations associated with the simplified treatment of the free surface and the thin-shear-layer approximation used. Second, the wave formation and thermocapillary Marangoni convection were not included in the analysis for the tub-like divertor. A "second approximation" analysis needs to be done in the future using full models and more sophisticated computer codes. At present, to our best knowledge, such computational tools are unavailable due to severe computational limitations associated with strong magnetic fields, high heat loads, complex flow geometry and related multi-effect phenomena that require a tight coupling between

the fluid flow and energy equations.[25] Significant progress in the analysis of free surface MHD flows can be expected in the future as soon as the present MHD computational tools evolve to the required level.

It should also be noted that the proposed designs don't cover many engineering details, which at this moment cannot be elaborated either. For example, we didn't consider the penetrations (ports) on the FW, for which special flow schemes need to be developed, where the MHD flows around the penetrations will most likely demonstrate essential 3-D features. Also, the practical problem of cooling the flow dividers needs to be resolved as the upper part of the dividers will most likely be exposed to plasma unless they are fully submerged in the liquid. The same issue applies to the flow deflectors.

To conclude, the proposed integrated concept of a LM flowing FW and open-surface divertor has been shown to have a wide design window, but these predictions were obtained using limited models and computational tools. Fundamental R&D for MHD free surface flows with internal and surface heating, are critically important to the further progress of the concept. This R&D effort should include full 3-D modeling and physical experiments for prototypic geometries and different conditions and flow parameters relevant to fusion.

ACKNOWLEDGMENTS

The study has been performed under U.S. Department of Energy Contracts DE-FG02-86ER52123 at UCLA and DE-AC52-07NA27344 at LLNL.

REFERENCES

1. B. O. KARASEV, I. V. LAVRENTEV, A. F. KOLESNICHENKO, O. A. LIELAUSIS, E. V. MURAVEV, V. N. DEMYANENKO, A. V. TANANAEV, "Research and Development of Liquid Metal Systems for a Tokamak Reactor," *Fusion Eng. Des*., **51**, 283–288 (1989).

2. M. ABDOU, A. YING, N. MORLEY, K. GULEC, S. SMOLENTSEV et al., "On the Exploration of Innovative Concepts for Fusion Chamber Technology – APEX Interim Report Overview," *Fusion Eng. Des*., **54**, 181–247 (2001).

3. R. E. NYGREN, T. D. ROGNLIEN, M. E. RENSINK, S. SMOLENTSEV, M. E. YOUSSEF et al., "A Fusion Reactor Design with a Liquid First Wall and Divertor, *Fusion Eng. Des*., **72**, 181-221 (2004).

4. M. SHIMADA, Y. HIROOKA, "Actively Convected Liquid Metal Divertor," *Nucl. Fusion*, **54**, 122002 (2014).

5. V. V. BURYAK, A. A. KOLESNICHENKO, A. F. KOLESNICHENKO, S. SMOLENTSEV, "Free-surface MHD Flows as a Potential Tool for High Heat Flux Removal in Fusion Applications," *Magnetohydrodynamics*, **48**, 651-666 (2012).

6. R. E. NYGREN, F. L. TABARES, "Liquid Surfaces for Fusion Plasma Facing Components—A Critical Review. Part I: Physics and PSI," *Nuclear Materials and Energy*, **9**, 6-21 (2016).

7. C. E. KESSEL, J. P. BLANCHARD, A. DAVIS, L. El-GUEBALY, N. GHONIEM et al., "The Fusion Nuclear Science Facility, the Critical Step in the Pathway to Fusion Energy," *Fusion Sci. Technol*., **68**, 225-236 (2015).

8. S. SMOLENTSEV, T. RHODES, G. PULUGUNDLA, C. COURTESSOLE, M. ABDOU, S. MALANG, M. TILLACK, C. KESSEL, "MHD Thermohydraulics Analysis and Supporting R&D for DCLL Blanket in the FNSF," *Fusion Eng. Des*., **135**, 314-323 (2018).

9. J. P. ALLAIN, C. N. TAYLOR, "Lithium-based Surfaces Controlling Fusion Plasma Behavior at the Plasma-material Interface," *Phys. Plasmas*, **19**, 056126 (2012).

10. L .E. ZAKHAROV, "Magnetic Propulsion of Intense Lithium Streams in a Tokamak Magnetic Field, *Phys. Rev. Lett*., **90**, 045001 (2003).

11. S. SMOLENTSEV, M. ABDOU, "Open-surface MHD Flow over a Curved Wall in the 3-D Thin-shear-layer Approximation," *Applied Mathematical Modelling*, **29**, 215-234 (2005).

12. T. D. ROGNLIEN, M. E. RENSINK, "Impurity Transport in Edge Plasmas with Application to Liquid Walls," *Phys. Plasmas*, **9**, 2120-2126 (2002).

13. T. D. ROGNLIEN, M. E. RENSINK, D. P. STOTLER, "Scrape-off Layer Plasma and Neutral Characteristics and their Interactions with Walls for FNSF," *Fusion Eng. Des*., **135**, 380-393 (2018).

14. B. D. NICHOLS, C. W. HIRT, "Calculating Three-dimensional Free Surface Flows in the Vicinity of Submerged and Exposed Structures," *J. Comp. Phys*., **12**, 234-246 (1973).

15. S. SMOLENTSEV, S. CUEVAS, A. BELTRAN, "Induced Electric Current-based Formulation in Computations of Low Magnetic Reynolds Number Magnetohydrodynamic Flows," J. Comput. Phys., **229,** 1558-1572 (2010).

16. S. SMOLENTSEV, "Mathematical Models for Magnetohydrodynamic Flows in a Fusion Reactor Blanket," *Plasma Dev. Oper*., **7**, 231-241 (1999).

17. G. O. ROBERTS, "Computational Meshes for Boundary Layer Problems." In: *Lecture Notes in Physics*, Vol. 8, New York, Springer-Verlag, 171-177 (1971).

18. F. G. BLOTTNER, "Variable Grid Scheme Applied to Turbulent Boundary Layers," *Comput. Meth. Appl. Mech. & Eng*., **4**, 179-194 (1974).

19. J. SOMMERIA, R. MOREAY, "Why, How and When MHD Turbulence Becomes Two-dimensional," *J. Fluid Mech*., **118**, 507-518 (1982).

20. JC. YANG, TY. QI, DW. REN, BQ. LIU, MJ. NI, "Rearrangement of Liquid Metal Surface Waves by a Uniform Transverse Magnetic Field," *Exp. Fluids*, **59** (2018), https://doi.org/10.1007/s00348-018-2617-x 2617-x.

21. J. C. TANNEHILL, D. A. ANDERSON, R. H. FLETCHER, Computational Fluid Mechanics and Heat Transfer, Taylor & Francis (1997).

22. A. ARAKAWA, "Computational Design for Long-term Numerical Integration of the Equations of Fluid Motion: Two-dimensional Incompressible Flow. Part I," *J. Comp. Phys*., **1**, 119-143 (1966).

23. M. GUPTA, "A Survey of Some Second-order Difference Schemes for the Steady-state Convection-diffusion Equation," *Int. J. Num. Meth. Fluids*, **3**, 319-331 (1983).

24. R. KAITA, R. MAJESKI, T. GRAY, H. KUGELl, D. MANSFIELD, J. SPALETA, et al., "Low Recycling and High Power Density Handling Physics in the Current Drive Experiment-Upgrade with Lithium Plasma-facing Components," *Phys. Plasmas*, **14**, 056111 (2007).

25. S. SMOLENTSEV, S. BADIA, R. BHATTACHARYAY, L. BUHLER, L. CHEN, Q. HUANG, et al., "An Approach to Verification and Validation of MHD Codes for Fusion Applications," *Fusion Eng. Des*., **100**, 65-72 (2015).

APPENDIX. MATHEMATICAL MODELS AND COMPUTER CODES

A numerical procedure employed in this study for the analysis of MHD flows and heat transfer utilizes two newly-developed numerical codes. The first code performs computations for the liquid FW. The velocity and temperature profiles at the exit of the FW flow obtained with the first code are then used as input data for the second code to solve the divertor problem. The two associated mathematical models include simplified MHD equations for the LM flow and the energy equation for the temperature field.

A. Liquid FW and Fast flow Divertor

A mathematical model developed in this study for a flowing thin layer of conducting fluid in a magnetic field can be used for both the liquid FW and the fast flow divertor. The key ideas are adopted from Ref. 11 where the governing equations are written in the 3-D boundary layer approximation (more general name is the thin-shear-layer approximation). While keeping the essential 3-D features, the present model neglects some terms associated with diffusion of momentum and heat in the main flow direction. The basis for this simplification is the order of magnitude scaling analysis that compares different terms in the equations. Typically, the convective transport in the main flow direction is dominant over the diffusion, providing the axial flow dimension is much larger compared to the cross dimension, i.e. if $h/L<<1$. In the case of the liquid FW or the fast flow divertor, where the flow thickness h~2 cm and the flow length L~10 m in the liquid FW and L~1 m in the divertor case , this assumption is obviously valid unless the flow experiences abrupt changes over a short distance of a few centimeters. This, for example, is the case of a so-called hydraulic jump, which cannot be fully analyzed within the boundary layer approximation. Dropping the diffusion terms in the equations results in a simplified model, which nevertheless preserves the most important flow features, but the associated computations are much faster compared to the full formulation. As reported in Ref. 11, a high Hartmann number computation (at Ha=8500) of a LM open-surface flow over a curved surface in the presence of a non-uniform magnetic field took only a few minutes using a personal computer. It should be noted that numerical calculations of simpler MHD flows that use full 3-D models, usually take tens of hours at much more moderate Hartmann numbers.

The special features of the proposed thin-shear-layer model can be seen from the momentum equation, which is written below in the scalar form with respect to the three velocity component V_1, V_2 and V_3 using orthogonal boundary fitted coordinates, such that x_1, x_2 and x_3 stand for the poloidal, radial and toroidal distances:

$$\frac{\partial V_1}{\partial t}+\frac{V_1}{H_1}\frac{\partial V_1}{\partial x_1}+V_2\frac{\partial V_1}{\partial x_2}+\frac{V_3}{H_3}\frac{\partial V_1}{\partial x_3}+\frac{1}{H_1H_3}\left(\frac{\partial H_1}{\partial x_3}V_1V_3-\frac{\partial H_3}{\partial x_1}V_3^2\right)=-\frac{1}{\rho}\frac{1}{H_1}\frac{\partial P}{\partial x_1}+g_1+\nu\frac{\partial^2 V_1}{\partial x_2^2}+\frac{1}{\rho}(\mathbf{j}\times\mathbf{B}^0)_1, \qquad (1)$$

$$\frac{L}{H_1^2}V_1^2+\frac{2M}{H_1H_3}V_1V_3+\frac{N}{H_3^2}V_3^2-g_2-\frac{1}{\rho}(\mathbf{j}\times\mathbf{B}^0)_2=-\frac{1}{\rho}\frac{\partial P}{\partial x_2}, \tag{2}$$

$$\frac{\partial V_3}{\partial t}+\frac{V_1}{H_1}\frac{\partial V_3}{\partial x_1}+V_2\frac{\partial V_3}{\partial x_2}+\frac{V_3}{H_3}\frac{\partial V_3}{\partial x_3}+\frac{1}{H_1H_3}\left(\frac{\partial H_3}{\partial x_1}V_1V_3-\frac{\partial H_1}{\partial x_3}V_3^2\right)=-\frac{1}{\rho}\frac{1}{H_3}\frac{\partial P}{\partial x_3}+g_3+\nu\frac{\partial^2 V_3}{\partial x_2^2}+\frac{1}{\rho}(\mathbf{j}\times\mathbf{B}^0)_3\cdot$$

(3)

The continuity equation reads:

$$\frac{1}{H_1H_3}\left[\frac{\partial(H_3V_1)}{\partial x_1}+\frac{\partial(H_1V_3)}{\partial x_3}\right]+\frac{\partial V_2}{\partial x_2}=0\cdot \tag{4}$$

Other equations that determine the induced electric current, which is needed to close the model, are not shown here but the interested reader can found them in Ref. 11. Equations (1-4) are based on the use of standard notions and operators in vector analysis and differential geometry. Here, $\mathbf{B^0}$ is the applied magnetic field, **j** is the induced electric current density, *t* is the time, **g** is the gravity vector, and *P* is the pressure. The parameters H_1, H_2 and H_3 are the metric coefficients, while *L*, *M* and *N* are the coefficients of the second fundamental form of the surface. These parameters are used to specify the geometry and curvature of the solid substrate behind the flowing liquid.

To close the model, the induced electric current **j** and the thickness of the liquid layer *h* need to be computed in parallel with the computations of the velocity and temperature as a function of time and spatial coordinates. To compute the flow thickness the "height function method" is employed, which limits the applicability of the model to relatively small changes in *h*.[14] This makes the model inapplicable in some special situations with large-amplitude disturbances, abrupt changes in the flow thickness and complex-shape interfaces such as overturning waves and surfaces with droplet formation. Another limitation of the model is that it doesn't describe possible detachments of the liquid layer from the solid substrate, when the retaining forces are not sufficiently strong. The flow detachment can however be roughly predicted based on a simple equation that compares the centrifugal (retaining) force and the gravity force component normal to the substrate that tries to tear the liquid layer from the wall in the upper part of the chamber.

To compute the electric currents, the induced magnetic field or electric potential need to be computed first and then the electric currents can be evaluated using Ampère's or Ohm's law. Another approach is computing the induced currents directly as proposed in Ref. 15. Under the specific designs, axisymmetric or sector, adopted in the present study as described above in Section II, further simplifications could be employed to avoid costly computations of the induced current. In the case of axisymmetric flows, the flow opposing Lorentz force arises from the interaction between the toroidal current and the radial magnetic field. The axisymmetric toroidal current can simply be computed from Ohm's law (for details see Ref. 11). In the case of the sector design, the strongest electric currents appear due to the interaction between the poloidal flow and the strong toroidal field component. They are largely closed in the cross-sectional plane in each sector. Under such conditions, all the equations can be averaged (integrated) between the two dividers.[16] In doing so, the cross-sectional electric current is eliminated but the associated flow opposing Lorentz force on the right hand side of the momentum equation remains included in the form of the so-called Hartmann breaking term, which is linearly dependent upon velocity. All the steps described above are routine, but associated derivations are bulky and thus are not shown here. The interested reader can find more details in Ref. 11.

A computer code is written in FORTRAN. The code computes a steady solution by advancing in time. A slug-type flow and constant flow thickness are used as an initial guess. All equations are approximated implicitly with finite-difference formulas using the finite-volume approach on a non-uniform mesh that clusters grid points near the solid substrate and free surface. The grid clustering is performed using the stretching transformation for the boundary-layer type of problems.[17] If the mesh is uniform, the finite-difference scheme provides the second-order approximation. The momentum equations (1) and (3) are of the marching type with respect to the poloidal coordinate x_1. At each time-step, these equations are solved using the Blottner-type technique, which had been developed for marching problems.[18] One computation takes typically a few minutes using a personal computer on a mesh that has 2001 (in poloidal direction) by 201 (in radial direction) points before reaching the steady-state.

B. Tub-like Divertor

The MHD flow in the tub divertor cannot be described using the boundary layer approximation because all three characteristic flow dimensions (poloidal, toroidal and radial) in the liquid pool are about the same. For example, in the deep tub design (Fig. 3a), the poloidal depth is 1.0 m, while the radial and toroidal dimensions are 1.2 m and 1.5 m correspondingly. As a result, the flow doesn't have one preferential direction such that all diffusion terms in the momentum and energy equation have to be retained. However, the governing equations can still be simplified. The physical basis for the simplification is a strong effect of the toroidal magnetic field, which tends to transform the flow to a special quasi-two-dimensional (Q2D) form.[19] In such a Q2D regime, the MHD flow demonstrates two very thin Hartmann boundary layers with the exponential variation of the velocity at the dividing walls and the core region. Most of the dissipation losses occur in the high velocity gradient Hartmann layers, while in the core region between the two Hartmann layers, the velocity and pressure almost don't vary along the magnetic field lines. After integrating the full 3-D equations with respect to the toroidal coordinate between the two dividers, the mathematical model simplifies to the following form:

$$\frac{\partial U}{\partial t}+U\frac{\partial U}{\partial x}+V\frac{\partial U}{\partial y}=-\frac{1}{\rho}\frac{\partial P}{\partial x}+\nu\left(\frac{\partial^2 U}{\partial x^2}+\frac{\partial^2 U}{\partial y^2}\right)-\frac{U}{\tau}, \tag{5}$$

$$\frac{\partial V}{\partial t}+U\frac{\partial V}{\partial x}+V\frac{\partial V}{\partial y}=-\frac{1}{\rho}\frac{\partial P}{\partial y}+\nu\left(\frac{\partial^2 V}{\partial x^2}+\frac{\partial^2 V}{\partial y^2}\right)-\frac{V}{\tau}-g+g\beta(T-T_0), \tag{6}$$

$$\frac{\partial U}{\partial x}+\frac{\partial V}{\partial y}=0, \tag{7}$$

$$\rho C_p\left(\frac{\partial T}{\partial t}+U\frac{\partial T}{\partial x}+V\frac{\partial T}{\partial y}\right)=k\left(\frac{\partial^2 T}{\partial x^2}+\frac{\partial^2 T}{\partial y^2}\right)+q'''. \tag{8}$$

These equation are written in terms of the core variables: *U(x,y)* and *V(x,y)* are the core velocity components in the radial-poloidal plane, *T(x,y)* is the averaged temperature and *P(x,y)* is the averaged pressure. Coordinates *x* and *y* stand for radial (horizontal) and poloidal (vertical) distances. Other notations, ρ, ν, σ, k, C_p, β stand for the fluid density, kinematic viscosity, electrical conductivity, thermal conductivity, specific heat, and the volumetric thermal expansion coefficient correspondingly; T_0

is a reference temperature; q''' is the volumetric heating; and $\tau = bB_{tor}^{-1}\sqrt{\rho/\sigma\nu}$ is the so-called "Hartmann braking time" (see Ref. 19), which is a time-scale of damping Q2D vortices due to ohmic and viscous losses in the Hartmann layers. The dimension *b* is half of the LM pool width in the toroidal direction and B_{tor} is the strength of the applied toroidal magnetic field, which in the present analysis is taken constant within each sector. The momentum equation is written in the Boussinesq approximation to include the buoyancy force. In our first analysis of the MHD flow in the tub divertor, we limit our considerations to a non-deformable free surface subject to thermocapillary tangential forces due to Marangoni convection. These forces appear due to the temperature gradients on the free surface, which cause gradients in the surface tension, which in turn drive the liquid on the surface to flow away from regions of low surface tension. With taking into account the Marangoni effect, the dynamic boundary condition at the free surface can be written as follows:

$$y = h: \quad -\mu\frac{\partial U}{\partial y} = \frac{1}{\gamma}\frac{\partial T}{\partial x}. \tag{9}$$

Here, $\mu = \nu\rho$ is the dynamic viscosity and γ is the temperature coefficient of surface tension. The assumption of non-deformable free surface needs to be verified in the future studies using a special free-surface tracking technique, for example, the volume of fluid method. However, the effect of the "wavy" interface on heat transfer might be found small because, in general, a magnetic field is known to have a strong damping effect on interfacial perturbations, especially on those of a small length scale (see Ref. 20), which are supposed to have a strongest influence on heat transfer. In addition to boundary condition (9), another one is needed for the temperature computations. This thermal boundary condition at free surface equates the radiative heat flux from the plasma q'' and the diffusive heat flux in the liquid at the interface:

$$y = h: \quad -k\frac{\partial T}{\partial y} = q''. \tag{10}$$

At the time of writing of this paper, the heat flux distributions for the tub divertor and also for other divertor options proposed in this study had not been evaluated. Because of this reason, our heat transfer analysis utilizes a model "bell-shaped" heat flux distribution with the peak of 10 MW/m^2.

To perform analysis, a computer code was developed in FORTRAN. Since the numerical algorithm is standard, only some basic ideas are presented here. To exclude the pressure, the governing equations (5-8) were first transformed into an equivalent form using vorticity and streamfunction as the main flow variables. The code solves the vorticity-streamfunction equations and the energy equation using a time-marching procedure (see e.g. Ref. 21). The governing equations were approximated implicitly with finite-difference formulas on a non-uniform mesh. The discretization is of second-order accuracy in time and space. Advancing in time is performed using the Adams-Bashforth scheme. Central-difference representations are used for the discretization of the diffusive terms. For the convective terms in the vorticity transport equation, three options are available: a central-difference scheme, a conservative scheme proposed by Arakawa (Ref. 22), and the Samarskii scheme (Ref. 23). At each time-step, the finite difference equations are solved using a tri-diagonal solver (see e.g. Ref. 21).

Special test studies were performed to evaluate a range of the numerical parameters in which the results are almost independent of the mesh size and the integration time step, and hence desired effects of the physical parameters can be observed. As a result of these tests, the number of mesh points was

chosen as 501 by 501 with clustering more points near the boundaries where higher velocity/temperature gradients can be expected compared to the flow bulk. The integration time step was also evaluated in several trials by comparing the instantaneous and time-averaged temperature distributions at several different Δt . As a result of these tests, the recommended dimensionless $\Delta t = 0.00001$, which was used in almost all computations for the Li divertor. The computational time needed to reach a statistical steady-state depends on the flow parameters and varies from hours to five-seven days using a personal computer. About 90% of the computational time is taken by solving the elliptic equation for the stream-function.